# Dependence of atmospheric transport into the Arctic on the meridional extent of the Hadley cell

**Huang Yang[1,4], Darryn, W. Waugh[1,2], Clara Orbe[3]and Gang Chen [4]**

[1]Department of Earth and Planetary Sciences, Johns Hopkins University, Baltimore, Maryland, USA
[2]School of Mathematics, University of New South Wales, Sydney, Australia
[3]NASA Goddard Institute for Space Studies, New York, New York, USA
[4]Department of Atmospheric and Oceanic Sciences, University of California, Los Angles, Los Angles, California, USA

**Key Points:**

- Transport of tracers from the northern midlatitude surface into the Arctic is sensitive to changes in the northern edge of the Hadley Cell
- The relative position between a tracer source and the Hadley Cell edge plays a major role in the transport into the Arctic
- Differences in the poleward transport are mainly due to differences in the near-surface mean flow rather than mixing in the free troposphere

Corresponding author: Darryn Waugh, `waugh@jhu.edu`

## Abstract

Recent studies have shown a large spread in the transport of atmospheric tracers into the Arctic among a suite of chemistry climate models, and have suggested that this is related to the spread in the meridional extent of the Hadley Cell (HC). Here we examine the HC–transport relationship using an idealized model, where we vary the mean circulation and isolate its impact on transport to the Arctic. It is shown that the poleward transport depends on the relative position between the northern edge of the HC and the tracer source, with maximum transport occurring when the HC edge lies near the middle of the source region. Such dependence highlights the critical role of near–surface transport by the Eulerian mean circulation rather than eddy mixing in the free troposphere, and suggest that variations in the HC edge and the tracer source region are both important for modeling Arctic composition.



## Plain Language Summary

Long–range transport plays a crucial role in determining the distribution of pollutants in the Arctic, as many pollutants have their sources in northern middle latitudes. Recent studies show large differences in transport into the Arctic among models and it has been suggested that this is related to differences in the northern edge of the Hadley Cell (HC) in the models. We revisit this topic using an idealized model in which the extent of the HC can be varied in a controlled manner. We show that the relative position between the tracer source and the northern edge of the HC plays an important role in determining how rapidly air is transported into the Arctic. The most rapid transport occurs when the HC edge lies near the middle of the tracer source region. This results suggest that variations in the HC edge and the tracer source region are both important for modeling Arctic composition.


## 1 Introduction

Trace gases and aerosols within the Arctic atmosphere are important for the Arctic climate and environment via impacts on radiation (AMAP, 2015a; Willis et al., 2018) and air quality (AMAP, 2006, 2015b). As these trace gases and aerosols originate primarily from lower latitudes, long–range meridional transport over the Northern Hemisphere (NH) extratropics is critical in determining their Arctic burdens and distributions (see Willis et al. (2018) and references therein). Therefore, improving our understandings of, and the ability to model, this meridional transport becomes essential for achieving a better assessment as well as prediction of the Arctic climate.

There is, unfortunately, large uncertainty in the simulated transport of tracers into the Arctic. This is highlighted by the large spread in simulated tracer mixing ratios in the Arctic from ensembles of chemistry transport or chemistry-climate models, with the multi-model spread approaching 100% of the ensemble mean for carbon monoxide CO and black carbon (Shindell et al., 2008), and 25–45% for idealized tracers (with simplified chemistry highlighting variations only in the transport) (Orbe et al., 2018; Yang et al., 2019). The causes of these inter-model differences are not known, and represent a major uncertainty in projections of changes in Arctic atmospheric composition.

Atmospheric transport of energy, moisture, and trace gases is often decomposed into a component due to the mean meridional circulation (MMC) and a component due to eddy mixing. Many previous studies have shown that eddy mixing dominates the climatological-mean transport into the Arctic (Peixoto & Oort, 1992; Shaw & Pauluis, 2012; Shen et al., 2017), and found robust temporal correlations between variations in eddy mixing and transport into the Arctic (Eckhardt et al., 2003, 2004;

Madonna et al., 2014; Liu & Barnes, 2015). Given these studies it would be reasonable to expect differences in eddy mixing between models to be the major contributor the large inter-model spread in transport into the Arctic. However, a recent study by Yang et al. (2019) (hereafter Y19) suggests that differences in the zonal–mean transport are instead the major cause of the differences in the transport into the Arctic among models.

Y19 examined the distribution of a CO50 tracer (a tracer with zonally asymmetric anthropogenic carbon monoxide (CO) emissions and a fixed chemical lifetime of 50 days) in models that participated in the Chemistry Climate Model Initiative (CCMI), and showed that models with a more northern Hadley Cell (HC) edge tend to have lower Arctic concentration of CO50. This occurs even for models that use (or are nudged to) meteorological fields from meteorological reanalyses. From this they suggested that the meridional extent of the HC, and its influence on the zonal–mean transport, is a key factor in the transport into the Arctic. Y19 also examined the distribution of a second tracer (NH50) with the same 50 day uniform lifetime but with a zonally uniform boundary condition. Surprisingly there is a weaker relationship between the Arctic concentration of NH50 and the HC extent, with even the opposite dependence during winter, i.e., increased Arctic NH50 for a wider HC. Y19 attributed the difference between CO50 and NH50 to the zonal extent of the NH50 sources and additional influence from differences in parameterized convection among the models (as shown earlier by Orbe et al. (2017, 2018)) that are primarily over the oceans during winter and thus become less important for land–based CO50.

The Y19 results are surprising, and have potential implications for simulations of present–day atmospheric composition and also for future projections. However, the analysis in Y19 was based on a rather small number of chemical models with many closely related, and there are differences in many other physical processes between the models in addition to their differences in the HC extent. Thus, it is not possible to make strong conclusions based just on this study, and it is therefore important to test the Y19 results in simulations where the HC is varied in a more controlled manner.

In this study, we perform such an analysis using an idealized model, where we can vary the mean atmospheric circulation and examine the response of tracer transport. The idealized model and simulations performed are described in Section 2. Section 3 examines the response of poleward transport to variations in the atmospheric circulations and highlight the importance of the relative position between the Eulerian mean circulation and tracer source region. Discussion and conclusions are in Section 4.

## 2 Models and Simulations

### 2.1 Idealized Model

We perform tracer simulations using the Geophysical Fluid Dynamical Laboratory (GFDL) spectral atmospheric dynamical core, which solves the dry primitive equations on the sphere with Newtonian relaxation towards a prescribed equilibrium temperature and Rayleigh friction in the planetary boundary layer (see Held and Suarez (1994) for details). The model is run at T42 horizontal resolution with 20 equally spaced sigma levels between $\sigma = 0.05$ and 1 (Chen et al., 2017). All model output are further interpolated into an isobaric coordinate with 23 ERA-40 levels to facilitate a more accurate flux calculation.

The radiative equilibrium temperature used in this study is

$$T_{\mathrm{eq}}\left(p,\phi\right) = \max\left\{200, \left[315 - 60\sin^2\phi - 10\log\left(\frac{p}{10^5}\right)\cos^2\phi - T'\right]\left(\frac{p}{10^5}\right)^{\kappa}\right\} \qquad (1)$$

where $\phi$ is the latitude, $p$ is the pressure, $\kappa = R/c_p = 2/7$ is the ratio of the gas constant of dry air $R$ to the specific heat capacity of dry air $c_p$, and

$$T' = \begin{cases} A\cos\left(2\phi - \frac{\pi}{2}\right)\sin\left(4\phi - \pi\right) & : \phi \geq 0 \\ 0 & : \phi < 0 \end{cases} \tag{2}$$

The $T'$ term is an addition to the orginial equilibrium temperature used in Held and Suarez (1994), and enables atmospheric states with different locations of the HC edge and jet to be formed (Garfinkel et al., 2013). To isolate the impacts of atmospheric circulations on tracer transport in just the NH, $T' = 0$ where $\phi < 0$.

Another important modification from Held and Suarez (1994) is the inclusion of a zonal wavenumber 2 surface geopotential height $\Phi_0$

$$\Phi_0\left(\lambda, \phi\right) = \max\left[0, gh_0 \sin^2\left(\frac{\phi - \phi_0}{\phi_1 - \phi_0}\pi\right)\cos(2\lambda + \pi)\right] \; : \phi_0 < \phi < \phi_1 \tag{3}$$

where $\lambda$ is the longitude, $g$ is the acceleration of gravity, $h_0 = 3$ km is the peak height of topography, and the southern and northern meridional bounds of the topography are $\phi_0 = 25°$N and $\phi_1 = 65°$N. The center of the topography is at 45°N which is collocated with the climatological jet location in the simulation with $T' = 0$. The topography helps reproduce a more realistic zonal structure of the NH jet with preferred maximum westerly over the Pacific and Atlantic Oceans and presumably more realistic transport by jet–related eddy mixing.

To test the sensitivity of poleward transport to the location of the HC edge, we perform seven different simulations with the parameter $A$ in Eq. 2 varying from -10 to 20, with an interval of 5. Fig.1 shows the variation in the HC (denoted by orange colors) for runs with $A = -10, 0,$ and 20 ($A = 0$ corresponds to the control flow in Held and Suarez (1994) except for the topography). The edge of the HC (hereinafter $\phi_{\mathrm{HC}}$) is calculated (as in Y19) as the latitude where the zonal–mean meridional flow $v$ averaged over 800–950 hPa equals 0 with southward flow to the south and northward flow to the north. $\phi_{\mathrm{HC}}$ varies from 17°N to 39°N as $A$ increases from -10 to 20 (bold gray lines in Fig 1), and we will refer to the simulations by this latitude (rather than $A$), i.e., simulations shown in Fig. 1 will be referred to as H17, H27, and H39. Note that the range of $\phi_{\mathrm{HC}}$ in the idealized model is much larger than the model spread in Y19 or interannual variations in reanalysis products (Moon & Ha, 2020). This large range was used so that we could fully test the sensitivity of the transport to $\phi_{\mathrm{HC}}$.

Although our main focus is to test the hypothesis of Y19 that the transport varies with $\phi_{\mathrm{HC}}$, Fig.1 shows that $\phi_{\mathrm{HC}}$ is not the only aspect of the circulation that change with $A$. There are changes in the strength and depth of the HC and the Ferrel Cell (FC) (blue colors), which are non-monotonic with $A$ . For $A$ increasing from -10 to 5 ($\phi_{\mathrm{HC}} = 17°$N to 31°N), there is a tendency for the HC to get weaker and shallower and the FC to get stronger and deeper. However, for $A > 5$ ($\phi_{\mathrm{HC}} > 31°$N) the changes in HC and FC strength and depth are small. The latitude of the midlatitude jet $\phi_{\mathrm{jet}}$ (vertical black line in Fig.1), defined as the latitude of the peak zonal winds at 850 hPa, also moves poleward as $A$ increases, but we will show later that variations in the poleward transport is unlikely due to the jet–related eddy mixing.

To examine the poleward transport in the different atmospheric flows, tracers are included in the simulations as in Chen et al. (2017) with a semi-Lagrangian scheme for horizontal advection (Lin et al., 1994), a finite–volume parabolic scheme for vertical advection, and no explicit numerical diffusion. For each of the different flows we include two tracers. Both tracers have fixed mixing ratio source between 20°N and 40°N within the bottom four layers of the model (approximately where pressure $p > 800$ hPa) and a

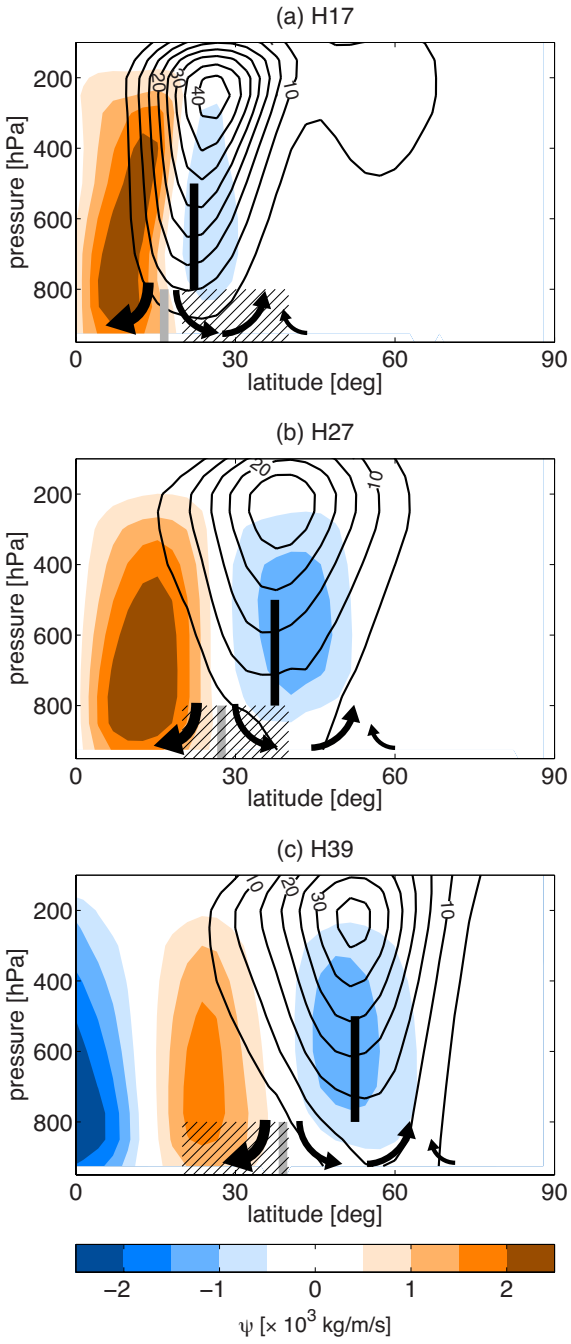


**Figure 1.** Latitude–altitude cross sections of zonal–mean atmospheric circulation for simulations with $A$ in Eq. 2 equal to (a) -10, (b) 0, and (c) 20, with corresponding northern edge of HC $\phi_{\mathrm{HC}}$ at 17°N, 27°N, and 39°N (gray vertical bars), respectively. Contours show the zonal wind (5 m/s interval) and shading shows the mass stream function $\psi$ (units: $\times 10^3$ kg/m/s). Orange shades denote the anti-cyclonic Hadley Cell whereas blue shades denote the cyclonic Ferrel Cell. The vertical black lines show the location of the jet ($\phi_{jet}$), the surface source region of ZS and ZA are marked by hatching, and the near–surface flow is shown as schematic arrows with arrow thickness denoting the flow strength.

uniform 50-day loss rate (which is the same loss as the CCMI CO50 and NH50 tracers, see below). However, the zonal variations of the mixing ratio between 20°N and 40°N differs between the tracers: For one tracer, referred to as the zonally symmetric (ZS) tracer, the surface mixing ratio is fixed at 1 mol/mol for all longitudes, whereas for the other tracer, the zonally asymmetric (ZA) tracer, the surface mixing ratio is fixed at 1 mol/mol only between 100–130°E. Comparison between the two tracers isolates the importance of the longitudinal distribution of tracer source for the transport to the Arctic. Since the tracers have a prescribed loss we do not include a global tracer–mass fixer (as was included in Chen et al., (2017). All simulations are integrated for 10 years. The tracers are introduced at the start of the fourth year and our analysis considers the last 6 years of the 10-year runs to avoid spin up in the dynamics and tracer transport.

### 2.2 CCMI Models

The results from the above idealized model simulations are compared with simulations of the CO50 and NH50 tracers from more comprehensive models that participated in Chemistry Climate Model Initiative (CCMI) (Eyring et al., 2013; Morgenstern et al., 2017). This suite of models includes models that calculate the meteorological fields within the model (chemistry-climate models), as well as models that use (or relax towards) meteorological fields from meteorological reanalyses (chemical transport or specified dynamics models). Both CO50 and NH50 have a fixed e-folding lifetime of 50 days and primary sources in the midlatitude boundary layer. However, their sources differ in the longitudinal distribution. NH50 has a zonally symmetric source at the bottom model level with fixed mixing ratio of $10^{-7}$mol/mol over 30–50°N while CO50 uses the annual-mean anthropogenic CO surface emissions at the year 2000 so that the CO50 source is zonally asymmetric across different continents with the maximum contribution from Asia over 20–40°N and secondary contributions from North America and Europe. We analyse the same 2000-2009 CO50 and NH50 simulations as studied in Y19 (see supplementary Table S1).

## 3 Results

### 3.1 Idealized Model

We first consider the tracer distribution for the three simulations shown in Fig.1 (H17, H27, and H39). For all three simulations, and for both ZS and ZA, the tracer distribution is qualitatively the same, see Fig. 2. The tracer mixing ratio is largest at the source region and decreases both poleward and equatorward of this region. Over the source region, the largest mixing ratios are at the surface, but further north the highest concentrations are above the surface. The height of the maximum increases with latitude until around $50-60$°N and north of this the highest mixing ratio remain around 500 hPa. This latitudinal variation in peak mixing ratios is similar to that of isentropic surfaces (thin gray contours), highlighting the importance of isentropic eddy mixing for the climatological–mean extratropical poleward tracer transport.

The climatological spatial distributions of the ZS and ZA resemble those of wintertime distributions of NH50 in CCMI models, see figure 1b of Orbe et al. (2018). This agreement includes the highest mixing ratios being above the surface for latitudes north of the source, and surfaces of constant mixing ratio approximately following an isentropic surface. There is also agreement with the CCMI CO50 simulations shown in figure 1e of Y19, although the largest Arctic CO50 occurs near the surface and not in the middle troposphere. This is possibly due to additional high latitude CO50 emissions over Europe that are transported into the Arctic along much lower isentropic surfaces. This difference notwithstanding, the general agreement of the distributions of ZS and ZA with NH50 and CO50 in more comprehensive models suggests that the

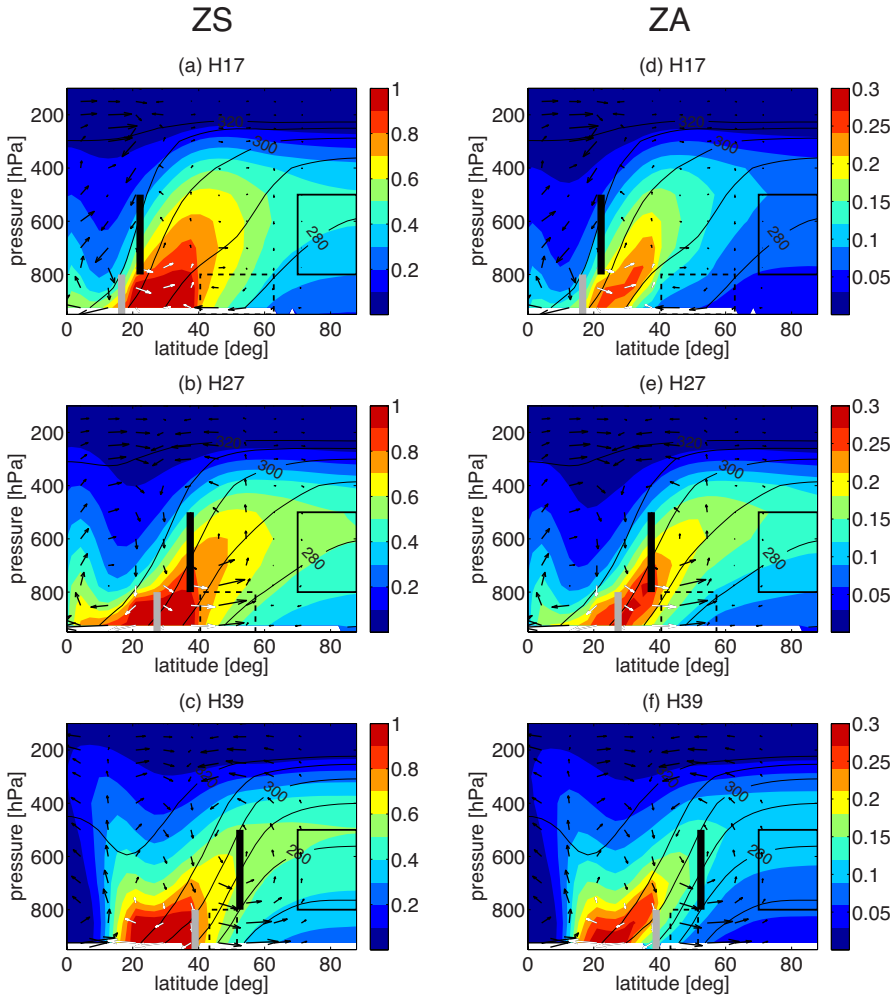


**Figure 2.** Zonal-mean tracer mixing ratio (colors), flow ($\bar{v}$ and $\bar{\omega}$ (vectors), and isentropic surfaces (gray thick contours) for (a-c) ZS and (d-f) ZA (d-f) tracers, for simulations shown in Fig. 1. Black and gray vertical lines show $\phi_{jet}$ and $\phi_{\mathrm{HC}}$, the black solid rectangle box denotes the Arctic mid-troposphere region (70–90°N, 500–800 hPa), and the black dashed rectangle denotes the near-surface midlatitude regions used in Fig. 4a,b.

idealized model is suitable to examine the dependence of tracer transport into the Arctic on $\phi_{\mathrm{HC}}$.

While there is qualitative agreement in the zonal–mean tracer distributions of ZS and ZA, there are noticeable differences in the magnitude of tracer mixing ratios north of 60°N. The highest Arctic mixing ratios (i.e., the maximum poleward transport) for the three simulations shown in Fig. 1 occur in the H27 simulation (see Fig. 2b). In this case, the $\phi_{\mathrm{HC}}$ (27°N) is slightly south of the midpoint of the tracer source region (30°N), and there is a strong northward flow over the northern half of the source region which results in strong near–surface horizontal transport out of the source region. For the H17 and H39 cases, there are lower Arctic mixing ratios, indicating weaker poleward transport. For H17 the $\phi_{\mathrm{HC}}$ is south of the source region, and poleward transport is largely suppressed by a weak meridional flow at the northern edge of the source despite that the source region is dominated by a northward flow in the lower branch of FC (Fig. 2a and schematic arrows in Fig. 1a). Whereas, for H39 the $\phi_{\mathrm{HC}}$

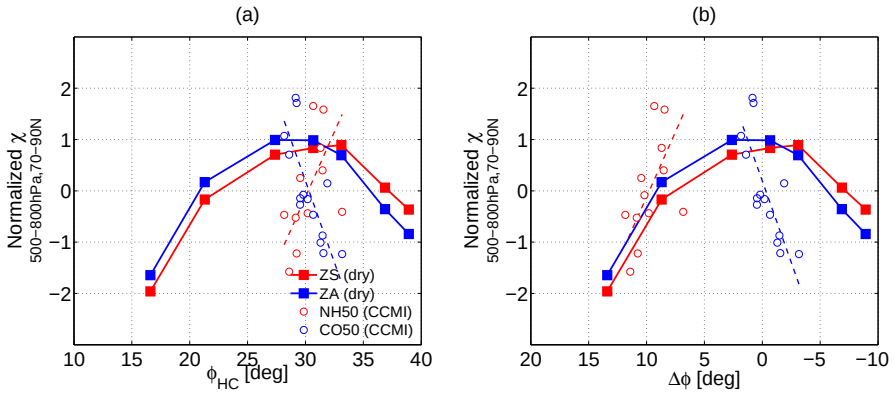


**Figure 3.** Response of normalized Arctic tracer concentration to variations in (a) the Hadley Cell edge $\phi_{\mathrm{HC}}$ and (b) $\Delta\phi$ the distance between the midpoint of tracer source and the Hadley Cell edge ($30^\circ - \phi_{\mathrm{HC}}$) . Solid symbols and lines show the results from the idealized model simulations of ZS (blue) and ZA (red). Open circled symbols show NH50 (red) and CO50 (blue) from the CCMI models, with regression lines shown as thin dashed lines

is at the northern edge of the source region and there is a strong equatorward flow throughout the source region, and weak poleward transport north from the source region (Fig. 2c and schematic arrows in Fig. 1c). In both cases, the surface tracer meridional gradient at the northern edge of the source region becomes larger, indicating less poleward transport out of the source region which leads to decreased Arctic mixing ratios.

The variation in Arctic mixing ratios is quantified by calculating the mixing ratio averaged over 70-90°N and 500-800 hPa (hereafter $\chi_{\mathrm{Arctic}}$). This region is used as it captures the location of the peak mixing ratios over the Arctic, and is the same region as used in Y19 enabling direct comparisons with their analysis. Fig. 3.1a shows the variation of $\chi_{\mathrm{Arctic}}$ with $\phi_{\mathrm{HC}}$ for the full suite of simulations. As the magnitudes of $\chi_{\mathrm{Arctic}}$ are different between ZS and ZA tracers and the relative difference in mixing ratios between different simulations is the most important, the mixing ratios are normalized for comparison. The normalization used is the difference in mixing ratio from mean mixing ratio over all simulations, divided by the standard deviation across all simulations. Fig. 3a shows that the maximum $\chi_{\mathrm{Arctic}}$ occurs when $\phi_{\mathrm{HC}} \sim 30^\circ$N, with decreasing $\chi_{\mathrm{Arctic}}$ as $\phi_{\mathrm{HC}}$ decreases to 17°N or increases to 39°N (as shown in Fig. 3). For simulations with $\phi_{\mathrm{HC}} \sim 30^\circ$N the southern half of tracer source (20–40°N) is within the HC while the northern half of source (proximity to the Arctic) is controlled by the FC featuring the maximum poleward transport. To explicitly show this relation between $\phi_{\mathrm{HC}}$ and the tracer source, we use the distance between the midpoint of tracer source region and the northern edge of the HC , $\Delta\phi = 30^\circ - \phi_{\mathrm{HC}}$, as an alternative coordinate, see Fig. 3b. The maximum poleward transport occurs when $\phi_{\mathrm{HC}}$ is near the midpoint of tracer source ($\Delta\phi \sim 0$), and the transport weakens as $\phi_{\mathrm{HC}}$ moves north or south of the midpoint of the source region (larger absolute value of $\Delta\phi$, i.e., $|\Delta\phi|$). Fig. 3 shows very similar responses for ZS and ZA, indicating that, without considering convective transport and its zonal asymmetry, the relative latitudinal position between tracer source and jet/mean circulations plays a more important role than the zonal distribution of tracer source for transport into the Arctic.

Examination of the tracer evolution in the simulations suggests that the poleward transport of the ZS and ZA tracers can be roughly divided into two stages. In the first stage, there is a near–surface horizontal movement from the subtropical source region

towards higher latitudes, and then in the second stage there is continuing poleward transport but now along isentropic surfaces. Analysis of the tracer mixing ratios in the near–surface midlatitude region bounded by the latitude of isentropes that also bound the Arctic mid-troposphere region (dashed boxes in Fig. 2) shows a variation with $\Delta\phi$ very similar to that of $\chi_{\text{Arctic}}$ (Fig. 4a,b). This suggests that variations in the Arctic tracer mixing ratios $\chi_{\text{Arctic}}$ in the middle and lower troposphere is mainly driven by variations in the first–stage transport, with additional contributions from variations in the structure of isentropic surfaces (i.e., isentropes in the Arctic intersect the ground at higher latitudes with larger meridional distance from the source in H17, see Fig. 2). The second stage of isentropic mixing, on the other hand, is very efficient as indicated by the coincidence between the tracer isopleths and isentropic surfaces, and therefore is likely to be less influenced by variations in the mid-latitude mean meridional circulations.

Above we have suggested that the near-surface meridional flow around the northern edge of the source region plays an important role in determinining the strength of poleward transport of tracers into the Arctic. Therefore, we explicitly examine the variation of the zonal-mean meridional velocity $v$ averaged over the region 800-950 hPa and 30-50°N. As shown in Fig. 4c, the meridional flow in this region also exhibits a non-monotonic response to changes in the relative position $\Delta\phi$, which is similar to that found for $\chi_{\text{Arctic}}$ for both ZS and ZA. This supports the suggestion that the meridional flow in this region is key for determining the efficiency of the tracer transport into the Arctic.

A similar non-monotonic dependence on $\Delta\phi$ is also found for the total tracer flux, defined as $\overline{v\chi}$ (where $\overline{(\,)}$ denotes the zonal mean), averaged over the 800–950hPa, 30–50°N region, see thick curves in Fig. 4d,e. Furthermore, by decomposing the total tracer flux into a zonal–mean component ($\bar{v}\,\bar{\chi}$) and an eddy component ($\overline{v'\chi'}$ where $'$ denotes the departure from zonal mean), it can be seen that the non-monotonic response of the total tracer flux to variation in $\Delta\phi$ is largely due to variations in the zonal–mean component with variations in the eddy component playing a secondary role (Fig. 4d,e). The above results are also valid for the tropospheric-column average in which effects of jet–related eddy mixing at higher altitudes is also considered (not shown). This is consistent with the suggestion by Y19 that the spread in transport into the Arctic among CCMI models is mainly due to variations in the near–surface transport by the Eulerian MMCs rather than transport in the free troposphere by jet–related eddy processes. It is, however, important to note that the eddy–related transport still plays a major role in contributing to the absolute magnitude of the transport (especially when there is large separation in the HC edge and source region).

As noted in Section 2, in addition to variations in $\Delta\phi$ there are variations in other aspects of the circulation (e.g. strength/depth of HC and FC). It is therefore possible that these characteristics, and not $\phi_{\text{HC}}$, could control the tracer transport into the Arctic. However, comparison of the Arctic tracer mixing ratios and the strength/depth metrics shows only weak relationships (see supplementary Fig. 1b-e), contrasting to the much better correlations between the Arctic tracer mixing ratios and $-|\Delta\phi|$ (equivalent to the non-monotonic response to variations in $\phi_{\text{HC}}$, see supplementary Fig. 1a). When $\phi_{\text{HC}}$ is south of the source mid-point ($\Delta\phi > 0$, H17 to H27 in Fig.1) there tends to be higher Arctic tracer mixing ratios with a stronger FC strength. However, when $\Delta\phi < 0$, there are weak changes in the strength/depth of the meridional circulations (also see in Fig. 1) which cannot explain the decrease in transport into the Arctic as $\phi_{\text{HC}}$ moving poleward. This indicates that $\phi_{\text{HC}}$ (and $\Delta\phi$) is the main aspect of the meridional circulation influencing the transport into the Arctic.

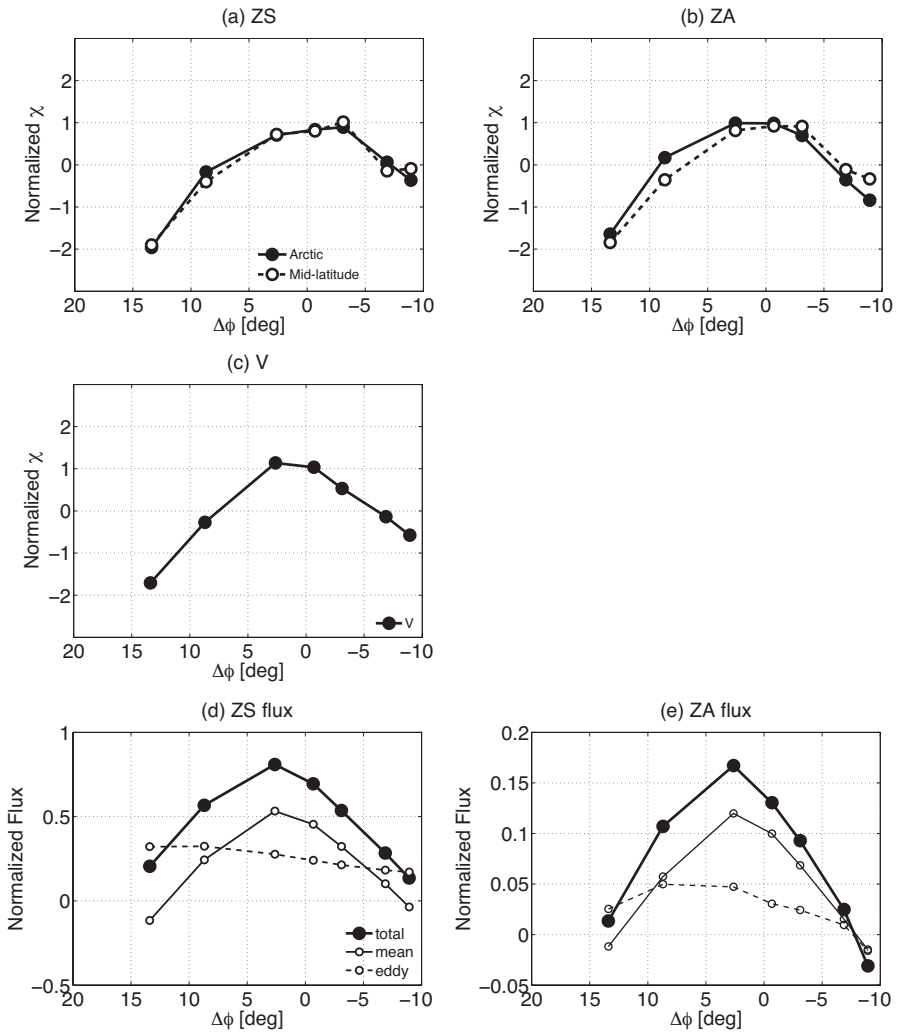


**Figure 4.** Variation of (a,b) normalized tracer concentrations, (c) near–surface zonal–mean meridional wind $v$, and (d,e) tracer fluxes with $\Delta\phi$. The tracer concentrations shown in (a,b) are averages over (solid) polar mid-troposphere and (dashed) midlatitude near–surface regions shown in Fig. 2. The meridional velocity and tracer fluxes in (c-e) are calculated over the NH midlatitude surface (30–50°N, 800–950 hPa). The tracer fluxes are also decomposed into a zonal–mean (thin solid) and an eddy component (thin dashed). Results for ZS tracer are shown on the left while those for ZA tracer are shown on the right.

### 3.2 CCMI Models

The main motivation for performing the idealized simulations is the Y19 analysis of CCMI models. We therefore compare the above variation of ZS and ZA tracers with those of the CCMI simulations of CO50 and NH50 tracers, to see if the idealized model results can help explain the variations found in the CCMI models. We focus on the CCMI tracer distributions during northern winter, as the idealized simulations are most representative during this season (due to absence of monsoonal circulation and stronger isentropic transport during this season).

As shown in Y19, there is a tendency for lower Arctic CO50 mixing ratios for CCMI models with more northern $\phi_{\mathrm{HC}}$ but the opposite tendency for NH50, see open symbols in Fig. 3a. It is important to note that the model spread and relationship with $\phi_{\mathrm{HC}}$ occurs for models using meteorological fields from reanalyses as well as for those calculating these fields internally. The tendency for lower Arctic CO50 for larger $\phi_{\mathrm{HC}}$ is consistent with our ZA and ZS simulations, but the increase in Arctic NH50 appears opposite to our simulations. However, when viewed in the coordinate of relative position $\Delta\phi$, there is agreement between our simulations and CCMI simulations for both CO50 and NH50, see Fig. 3b. Note, that the x-axis has been reversed in panel (a). This occurs because the source of the NH50 (30–50°N) is north of the HC edge in the CCMI models and $\Delta\phi > 0$. The increase in Arctic NH50 for a more northern $\phi_{\mathrm{HC}}$ is then consistent with the increase in ZS and ZA for decreased $\Delta\phi$. In contrast, the main source region for CO50 ($\sim$ 20–40°N) is around or south of the HC edge (i.e., $\Delta\phi < 0$, so the decrease in Arctic CO50 with more northern $\phi_{\mathrm{HC}}$ in the CCMI models is also consistent with the ZS and ZA tracers in the region where $\Delta\phi < 0$. Although there is general agreement between the CO50 and ZS/ZA variations with $\Delta\phi > 0$, there are quantitative differences. These could be due to differences in the sources of the different tracers or differences in the transport between the idealized and comprehensive models.

Y19 speculated that the different sensitivity of NH50 from CO50 in response to variations in the HC edge was due to the NH50 source region longitudinally including oceans, and its transport being primarily impacted by convection over oceans which plays less of a role for land–based tracers like CO50. However, the simulations here suggest that difference in the latitude of the source region CO50 and NH50 can mainly explain the differences in the sensitivity of their wintertime transport to the HC edge.

## 4 Discussions and Conclusions

The sensitivity of transport from the midlatitude surface towards the Arctic mid-troposphere to the meridional extent of the Hadley Cell (HC) has been examined using an idealized atmospheric model that includes idealized tracers. It is shown that the rate of the poleward transport depends on the $\Delta\phi$, the distance between the midpoint of the source region and the northern edge of the HC $\phi_{\mathrm{HC}}$, with Arctic tracer concentration varying non-monotonically with $\Delta\phi$. The maximum poleward transport occurs when $\Delta\phi \sim 0$ and there is a strong poleward surface flow over the northern edge of the source region. If $\Delta\phi > 10°$ ($\phi_{\mathrm{HC}}$ is south of the source region), there is a much weaker poleward transport over the source region resulting in lower Arctic mixing ratios. At the other extreme, if $\Delta\phi < -5°$ ($\phi_{\mathrm{HC}}$ is at the northern edge of the source region) the HC lies over the source region with a strong equatorward surface flow and therefore suppresses poleward transport over the source region.

The non-monotonic variation in the transport into the Arctic with $\Delta\phi$ in our idealized simulations helps explain the differing sensitivity of Arctic CO50 and NH50 to variations in the HC edge among the chemical-transport and chemistry-climate models reported in Y19. For all models the wintertime $\phi_{\mathrm{HC}}$ is south of the midpoint

of the NH50 source region (i.e., $\Delta\phi > 0$ for NH50) but $\phi_{\mathrm{HC}}$ is around or north of the midpoint of the major CO50 source region (i.e., $\Delta\phi < 0$ for CO50). Consistent with our idealized similations, for models with a more northern $\phi_{\mathrm{HC}}$ there is an increase in Arctic NH50 (as in $\Delta\phi > 0$ regime) but a decrease in Arctic CO50 (as in $\Delta\phi < 0$ regime). In other words, our simulations support the hypothesis of Y19 that differences in $\phi_{\mathrm{HC}}$ among models is a major contributor to the spread in simulated transport into the Arctic.

Our analysis supports the Y19 conjecture that HC–related variations in the Eulerian zonal–mean transport near the surface rather than jet–related eddy mixing in the free troposphere plays the most important role in causing variations in transport into the Arctic mid-troposphere among chemistry-climate and chemical transport models. In the idealized model the poleward tracer transport can be divided into an initial stage with primarily near–surface horizontal transport from the source to higher latitudes followed by transport along isentropic surfaces into the Arctic mid-troposphere. Variations in the meridional extent of the HC between simulations cause large differences in transport in the first stage, which dominate the differences in the Arctic mixing ratios in the idealized model. Tracer flux decomposition further indicates that differences of transport in the first stage are largely driven by differences in the Eulerian zonal–mean transport.

This does not, however, mean that eddies play a minor role for poleward transport. Despite weaker contribution to variations in the poleward transport between models, eddies are still the dominant contributor to the climatological magnitude of poleward transport and could also be the dominant contributor to temporal variations in poleward transport. Moreover, if mean and eddy transport is defined in the transformed Eulerian mean framework where mean circulation is an approximation to the Lagrangian circulation, eddy becomes the more important factor than mean circulation for variations in the poleward transport given the essential role of eddy–driven Ferrel cell in the conventional Eulerian mean framework (not shown). Therefore, it is less meaningful to argue which is the best way to differentiate between mean and eddy transport near surface but rather this study highlights more on the critical region for poleward transport of surface pollutants into the Arctic. That is, the role of near–surface transport by the Eulerian MMCs in the first stage rather than the isentropic transport in the free troposphere by strong eddy mixing in the second stage.

The results in this paper are subject to several limitations, including that we have only considered tracers with chemical lifetimes of a few months that originate from the northern midlatitude surface, have not included convection-related transport, and have focused on mid-tropospheric Arctic tracer mixing ratios. However, the fact that both comprehensive and idealized models (i.e., results of Y19 and this study) indicate that the separation of the source region and edge of the HC is an important factor in the transport into the Arctic, and suggests that this should be taken into consideration in studies of future changes in Arctic composition. Future changes in either of the location of trace gas sources or the HC edge could impact transport into the Arctic. A large number of modeling studies show a tropical expansion and poleward shift of MMCs as the climate continues to warm (except perhaps during summer over the Pacific (Shaw & Voigt, 2015)). At the same time, there will likely continue to be a southward shift of NH pollutant emissions with drastically increased emissions in low-latitude developing countries (Patra et al., 2011). The impact of these two movements may lead to a scenario with less efficient transport into the Arctic. Further studies, using idealized and comprehensive models, are needed to examine this possibility.

## Acknowledgments

We thank the Centre for Environmental Data Analysis (CEDA) for hosting the CCMI data archive. We acknowledge the modeling groups for making their simulations avail-

able for this analysis and the joint WCRP SPARC/IGAC ChemistryClimate Model Initiative (CCMI) for organizing and coordinating this model data analysis activity. In addition, Clara Orbe wants to acknowledge the high- performance computing resources provided by the NASA Center for Climate Simulation (NCCS) and support from the NASA Modeling, Analysis and Prediction (MAP) program. Huang Yang and Darryn W. Waugh acknowledge support from NSF grants AGS-1403676. Darryn W. Waugh acknowledges NSF grant and AGS-131876 and NASA grant NNX14AP58G. Gang Chen is supported by NSF grant AGS-1742178. Model output from the GFDL dry dynamical core is archived on the Johns Hopkins University Data Archive at https://archive.data.jhu.edu/dataverse/root while CCMI model output are available at ftp.ceda.ac.uk and www.earthsystemgrid.org.

## References

AMAP. (2006). *Arctic Pollution 2006: Acidification and Arctic Haze*. Oslo, Norway. Retrieved from `http://www.amap.no/documents/doc/arctic-pollution-2006/70`

AMAP. (2015a). *AMAP Assessment 2015: Black carbon and ozone as Arctic climate forcers* (Tech. Rep.). Oslo, Norway. Retrieved from `https://www.amap.no/documents/doc/amap-assessment-2015-black-carbon-and-ozone-as-arctic-climate-forcers/1299`

AMAP. (2015b). *AMAP Assessment 2015: Human Health in the Arctic* (Tech. Rep.). Oslo, Norway. Retrieved from `https://www.amap.no/documents/doc/amap-assessment-2015-human-health-in-the-arctic/1346`

Andrews, D. G. (1976). Planetary waves in horizontal and vertical shear: The generalized Eliassen-Palm relation and the mean zonal acceleration. *Journal of Atmospheric Sciences*, *33*(11), 2031–2048.

Bowman, K. P., & Erukhimova, T. (2004). Comparison of global-scale Lagrangian transport properties of the NCEP reanalysis and CCM3. *Journal of Climate*, *17*(5), 1135–1146. doi: 10.1175/1520-0442(2004)017⟨1135:COGLTP⟩2.0.CO;2

Chen, G., Orbe, C., & Waugh, D. (2017). The role of monsoon-like zonally asymmetric heating in interhemispheric transport. *Journal of Geophysical Research: Atmospheres*, *122*, 3282–3298. doi: 10.1002/2016JD026427

Chen, G., & Plumb, A. (2014). Effective Isentropic Diffusivity of Tropospheric Transport. *Journal of Atmospheric Sciences*, *71*, 3499–3520. doi: 10.1175/JAS-D-13-0333.1

Eckhardt, S., Stohl, A., Beirle, S., Spichtinger, N., James, P., Forster, C., ... Jennings, S. G. (2003). The North Atlantic Oscillation controls air pollution transport to the Arctic. *Atmospheric Chemistry and Physics*, *3*(5), 1769–1778. doi: 10.5194/acp-3-1769-2003

Eckhardt, S., Stohl, A., Wernli, H., James, P., Forster, C., & Spichtinger, N. (2004). A 15-year climatology of warm conveyor belts. *Journal of Climate*, *17*(1), 218–237. doi: 10.1175/1520-0442(2004)017⟨0218:AYCOWC⟩2.0.CO;2

Eyring, V., Lamarque, J.-F., Hess, P., Arfeuille, F., Bowman, K., Chipperfield, M. P., ... Young, P. J. (2013). Overview of IGAC/SPARC Chemistry-Climate Model Initiative (CCMI) Community Simulations in Support of Upcoming Ozone and Climate Assessments. *SPARC Newsletter*, *40*(January), 48–66. Retrieved from `http://www.met.reading.ac.uk/ccmi/?page{\_}id=15` doi: SPARCNewsletterNo.40,p.48-66,2013

Garfinkel, C. I., Waugh, D. W., & Gerber, E. P. (2013). The effect of tropospheric jet latitude on coupling between the stratospheric polar vortex and the troposphere. *Journal of Climate*, *26*(6), 2077–2095. doi: 10.1175/JCLI-D-12-00301.1

Held, I. M., & Suarez, M. J. (1994). A Proposal for the Intercomparison of the Dynamical Cores of Atmospheric General Circulation Models. *Bul-*

*letin of the American Meteorological Society*, *75*(10), 1825–1830. doi: 10.1175/1520-0477(1994)075⟨1825:apftio⟩2.0.co;2

Lin, S.-J., Chao, W. C., Sud, Y. C., & Walker, G. K. (1994). *A class of the van Leer-type transport schemes and its application to the moisture transport in a general circulation model* (Vol. 122) (No. 7). doi: 10.1175/1520-0493(1994)122⟨1575:acotvl⟩2.0.co;2

Liu, C., & Barnes, E. A. (2015). Extrememoisture transport into the Arctic linked to Rossby wave breaking. *Journal of Geophysical Research*, *120*(9), 3774–3788. doi: 10.1002/2014JD022796

Liu, C., & Barnes, E. A. (2018). Quantifying isentropic mixing linked to Rossby wave breaking in a modified Lagrangian coordinate. *Journal of the Atmospheric Sciences*, *75*(3), 927–942. doi: 10.1175/JAS-D-17-0204.1

Madonna, E., Wernli, H., Joos, H., & Martius, O. (2014). Warm conveyor belts in the {ERA}-{I}nterim dataset (1979-2010). {P}art I: climatology and potential vorticity evolution. *Journal of Climate*, *27*(1990), 3–26. doi: 10.1175/JCLI-D-12-00720.1

Moon, H., & Ha, K. J. (2020). Distinguishing changes in the Hadley circulation edge. *Theoretical and Applied Climatology*, *139*(3-4), 1007–1017. doi: 10.1007/s00704-019-03017-1

Morgenstern, O., Hegglin, M., Rozanov, E., O'Connor, F., Luke Abraham, N., Akiyoshi, H., ... Zeng, G. (2017). Review of the global models used within phase 1 of the Chemistry-Climate Model Initiative (CCMI). *Geoscientific Model Development*, *10*(2), 639–671. doi: 10.5194/gmd-10-639-2017

Orbe, C., Newman, P. A., Waugh, D. W., Holzer, M., Oman, L. D., Li, F., & Polvani, L. M. (2015). Airmass origin in the Arctic. Part I: Seasonality. *Journal of Climate*, *28*(12), 4997–5014. doi: 10.1175/JCLI-D-14-00720.1

Orbe, C., Waugh, D., Newman, P. A., & Steenrod, S. (2016). The Transit-Time Distribution from the Northern Hemisphere Midlatitude Surface. *Journal of the Atmospheric Sciences*, *73*, 3785–3802. doi: 10.1175/JAS-D-15-0289.1

Orbe, C., Waugh, D. W., Yang, H., Lamarque, J. F., Tilmes, S., & Kinnison, D. E. (2017). Tropospheric transport differences between models using the same large-scale meteorological fields. *Geophysical Research Letters*, *44*(2), 1068–1078. doi: 10.1002/2016GL071339

Orbe, C., Yang, H., Waugh, D. W., Zeng, G., Morgenstern, O., Kinnison, D. E., ... Oman, L. D. (2018). Large-scale tropospheric transport in the Chemistry-Climate Model Initiative (CCMI) simulations. *Atmos. Chem. Phys*, *185194*(March), 7217–7235. Retrieved from `https://www.atmos-chem-phys.net/18/7217/2018/acp-18-7217-2018.pdf` doi: 10.5194/acp-18-7217-2018

Patra, P. K., Houweling, S., Krol, M., Bousquet, P., Belikov, D., Bergmann, D., & Bian, H. (2011). TransCom model simulations of CH4 and related species: linking transport, surface flux and chemical loss with CH4 variability in the troposphere and lower stratosphere. *Atmospheric Chemistry and Physics*, *11*, 12813–12837. doi: 10.5194/acp-11-12813-2011

Peixoto, J. P., & Oort, A. H. (1992). *Physics of Climate*. American Insititute of Physics.

Polvani, L. M., & Esler, J. G. (2007, dec). Transport and mixing of chemical air masses in idealized baroclinic life cycles. *Journal of Geophysical Research*, *112*(D23), D23102.

Shaw, T. A., & Boos, W. R. (2012). The tropospheric response to tropical and subtropical zonally-asymmetric torques : Analytical and idealized numerical model results. *Journal of the Atmospheric Sciences*, *69*(1), 214–235.

Shaw, T. A., & Pauluis, O. (2012). Tropical and Subtropical Meridional Latent Heat Transports by Disturbances to the Zonal Mean and Their Role in the General Circulation. *Journal of the Atmospheric Sciences*, *69*(6), 1872–1889. doi: 10.1175/jas-d-11-0236.1

513 Shaw, T. A., & Voigt, A. (2015). Tug of war on summertime circulation between
514 radiative forcing and sea surface warming. *Nature Geoscience*, *8*(7), 560–566.
515 doi: 10.1038/ngeo2449
516 Shen, Z., Ming, Y., Horowitz, L. W., Ramaswamy, V., & Lin, M. (2017). On the sea-
517 sonality of arctic black carbon. *Journal of Climate*, *30*(12), 4429–4441. doi: 10
518 .1175/JCLI-D-16-0580.1
519 Shindell, D. T., Chin, M., Dentener, F., Doherty, R. M., Faluvegi, G., Fiore, A. M.,
520 ... Zuber, A. (2008). A multi-model assessment of pollution transport to
521 the Arctic. *Atmospheric Chemistry and Physics*, *8*(17), 5353–5372. Re-
522 trieved from `http://www.atmos-chem-phys.net/8/5353/2008/` doi:
523 10.5194/acp-8-5353-2008
524 Stohl, A. (2006). Characteristics of atmospheric transport into the Arctic tropo-
525 sphere. *Journal of Geophysical Research*, *111*(D11306), 1–17. doi: 10.1029/
526 2005JD006888
527 Willis, M. D., Leaitch, W. R., & Abbatt, J. P. D. (2018). Processes Controlling
528 the Composition and Abundance of Arctic Aerosol. *Reviews of Geophysics*, *56*,
529 621–671. doi: 10.1029/2018RG000602
530 Yang, H., Waugh, D. W., Orbe, C., Zeng, G., Morgenstern, O., Kinnison, D. E., ...
531 Schofield, R. (2019). Large-scale transport into the Arctic: the roles of the
532 midlatitude jet and the Hadley Cell. *Atmospheric Chemistry and Physics*, *19*,
533 5511–5528. doi: 10.5194/acp-2018-841